Supporting Information for

Supramolecular Cyclization of Semiflexible Cylindrical Micelles Assembled from Rod-Coil Graft Copolymers

Liang Gao, Rui Hu, Pengfei Xu, Jiaping Lin, Liangshun Zhang, and Liquan Wang**

Shanghai Key Laboratory of Advanced Polymeric Materials, Key Laboratory for Ultrafine Materials of Ministry of Education, School of Materials Science and Engineering, East China University of Science and Technology, Shanghai 200237, China

Contents

1. Simulation Method and Model

1.1 Brownian Dynamics (BD) Simulation

We considered the simulation system consisting of rod-coil graft copolymers in implicit solvents. The graft copolymer comprises a rigid backbone, multiple pendant groups, and two side chains, as shown in Figure 1a. The graft copolymer was modeled as $\mathbf{R_m}$-*g*-$(\mathbf{C_n})_2$, where **R** (green beads) and **C** (red beads) denote the rigid backbone and side chain, respectively, and the subscripts **m** and **n** denote the bead numbers. The **P** bead, representing the pendant group of backbone, is jointed to each **R** bead.

The bead-bead interactions are given by the bonding potential U_{mol} and the nonbonding potential U_{ij}. The U_{mol} can maintain a desired molecular chain structure, while the U_{ij} describes the nonbonding interactions. For the rod backbone, the U_{mol} is divided into two parts, that is, the bond stretching potential U_{bond} and the angle bending potential U_{angle}. All the neighboring beads are connected by a bond modeling with a harmonic spring potential given by

$$U_{bond}(r) = \frac{1}{2} k_b (r - r_0)^2 \tag{S-1}$$

where k_b is the bond spring constant, r is the distance between two bonded beads, and r_0 is the equilibrium bond length. To model the rigidity of the rod backbones, the angle bending potential is introduced

$$U_{angle}(\theta) = \frac{1}{2} k (\theta - \theta_0)^2 \tag{S-2}$$

where k_a is the angle spring constant, θ is the angle between two neighboring bonds, and θ_0 is the equilibrium angle.

The nonbonding potential U_{ij} between *i*-th and *j*-th beads is given by the standard Lennard-Jones (LJ) potential

$$U_{ij} = \begin{cases} 4\varepsilon_{ij}\left[\left(\dfrac{\sigma}{r_{ij}}\right)^{12} - \left(\dfrac{\sigma}{r_{ij}}\right)^{6} - \left(\dfrac{\sigma}{r_{ij}^c}\right)^{12} + \left(\dfrac{\sigma}{r_{ij}^c}\right)^{6}\right], & r \le r_{ij}^c \\ 0, & r > r_{ij}^c \end{cases} \tag{S-3}$$

where $r_{ij} = \left|\mathbf{r}_i - \mathbf{r}_j\right|$ with $\mathbf{r}_i$ and $\mathbf{r}_j$ being the positions of the *i*-th and *j*-th beads, respectively. r_{ij}^c is the cut-off distance and ε_{ij} is the interaction strength.

The simulations were performed by applying the simulator, coarse-grained molecular dynamics program based on LAMMPS.[S1] All the simulations were performed in a cubic cell using a dynamic algorithm with the temperature controlling method (NVT ensemble). Brownian dynamics (BD) simulation, which was developed by Grest and Kremer, is used because of the implicit description of continuum solvent and the simplification of internal motions.[S2] The temporal evolution of the beads obeys the Langevin equation, including all the potentials, the friction term, and the noise term. The beads are coupled to a heat bath, and the equation of motion is written as

$$m_i \frac{d^2\mathbf{r}_i}{dt^2} = \mathbf{F}_i - \Gamma_0 \frac{d\mathbf{r}_i}{dt} + \mathbf{W}_i(t) \tag{S-4}$$

where m_i is the mass of the i-th bead, Γ_0 is the friction constant, and $\mathbf{F}_i$ is the force acting on the i-th bead calculated by the potentials consisting of U_{mol} and U_{ij}. $\mathbf{W}_i(t)$ is calculated through the following fluctuation-dissipation relation:

$$\left\langle \mathbf{W}_i(t) \cdot \mathbf{W}_j(t') \right\rangle = 6k_{\mathrm{B}}T\Gamma_0\delta_{ij}\delta(t-t') \tag{S-5}$$

The periodic boundary conditions were imposed. The integration time step Δt = 0.005τ, and the simulation temperature $k_{\mathrm{B}}T$ = 3.0ε was selected. Here, $\tau = (m\sigma^2/\varepsilon)^{1/2}$ is the time unit, m is the unit of mass, σ is the unit of length, and ε is the unit of energy.

1.2 Setting of Parameters

Junction Point. To model the graft copolymer with random grafted side chains, the junction points on the backbone were chosen randomly for grafting the coil chains. Figure S1 shows the probability distribution of junction points on the backbones of $\mathbf{R}_{12}$-g-$(\mathbf{C}_6)_2$, which is the statistical result of 200 graft copolymers. The distribution shown in Figure S1 confirms the randomness of the junction points.

Bond and Angle. All the neighboring beads are connected by a bond modeling with a harmonic spring potential, which is given by Eq. S-1. The equilibrium bond length r_0 is 1.5σ, 1.5σ, and 0.75σ for rigid backbone, grafted side chain, and pendant group, respectively. We defined the bond length on the backbone as b and the bond length between backbone bead and pendant group as c. The value of k_b set as 100ε to avoid the over-stretching of bonds. To model the rigidity of the rod backbones,

the angle bending potential is introduced by Eq. S-2. In this equation, $\theta_0 = 180°$ and the k value is varied to describe the backbone rigidity.[S3-S5] For the coil grafted chains, $k = 0$.

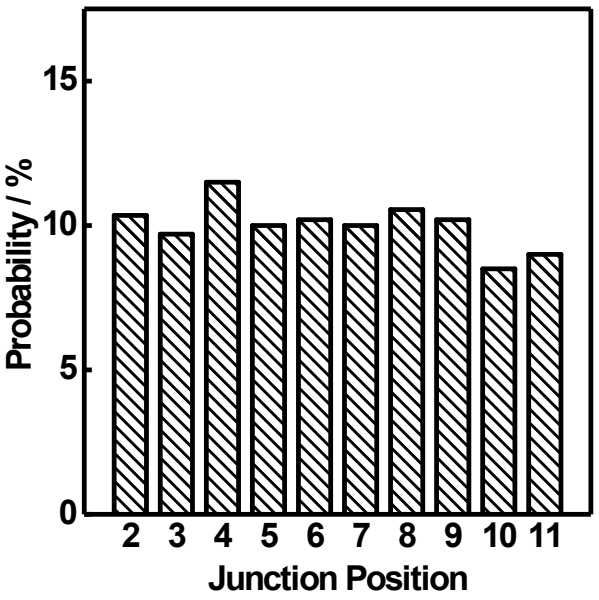

Figure S1. Probability distribution of junction points on the backbones of $\mathbf{R}_{12}$-*g*-$(\mathbf{C}_6)_2$.

Cut-Off Radius. To account for the solvent selectivity, the cut-off distances of the LJ potential Eq. (S-3) for graft copolymers is defined as follows. For the hydrophilic **C** side chains, the **C** beads are purely repelled with each other by setting r_{CC}^c to be $2^{1/6}\sigma$. To simulate the immiscibility between hydrophilic and hydrophobic blocks, r_{RC}^c and r_{PC}^c were also set to be $2^{1/6}\sigma$. While for the hydrophobic beads, the **R** beads (and **P** beads) can be attracted with each other by setting r_{RR}^c (and r_{PP}^c) to be 2.5σ. Moreover, the r_{RP}^c is 2.5σ to keep the stable junction of pendant groups.[S3-S5]

Interaction Strength. In the first-step assembly, for the **C**−**C**, **R**−**C**, and **P**−**C** repulsive interactions, the interaction strengths were set as $\varepsilon_{CC} = \varepsilon_{RC} = \varepsilon_{PC} = 1.0\varepsilon$. For the short-range attractive interaction, the interaction strength between **R**−**R** beads was set as 3.5ε, and those of **P**−**P** interaction and **R**−**P** interaction were set as 1.0ε. These parameter settings are corresponding to the addition of selective solvent (water) and the aggregation of graft copolymers in the experiments. In the cyclization stage, we increased the interaction strength ε_{PP} from 1.0ε to 5.0ε, corresponding to the constriction of PBLG pendant groups after adding THF in the experiments.[S3-S5] All the interaction strengths ε_{ij} between i-th and j-th beads are given in Table S1.

Table S1. Interaction strengths ε_{ij} used in BD simulations

ε_{ij}	**R**	**P**	**C**
R	3.5	1.0	1.0
P		1.0→5.0	1.0
C			1.0

Simulation Time. In the first-step assembly, 1.0×10^7 BD steps ($5.0 \times 10^4\tau$) were carried out so that the computing time is long enough for the system to achieve an equilibrium state. In the simulation of the cyclization stage, 1.0×10^7 BD steps ($5.0 \times 10^4\tau$) were also carried out. The simulation time is long enough for the systems to achieve the equilibrium.

1.3 Characterization of Orientational Angle

We present a mathematical method to describe the orientation of rod backbones in the micelle cores. As we defined in our previous work,[S3-S5] the orientation angle ϕ is the angle between the normalized vector of the rod block $\mathbf{u}_i$ and the normalized vector of chosen direction $\mathbf{u}_\mathrm{d}$, expressed as $\cos(\phi) = \mathbf{u}_i \cdot \mathbf{u}_\mathrm{d}$. For the cylindrical micelles, the chosen direction vector is the long axis of cylindrical micelles. For the toroidal micelles, this direction vector is the tangent vector of the toroid.

1.4 Records of Energy Variations in the Cyclization Process

To analyze the variation of energy as a function of self-assembly times, the angle potential of the backbones and the LJ potentials for all the pairwise interactions were recorded. The energy variation ΔE_{ij} from the cylindrical micelle to the cyclized micelle was calculated. The energy variations shown in Figure 3 are the time-average values of the chosen pairwise interactions. The bending energy was calculated from the angle potential (Eq. S-2) of the backbones.

2. Experimental Section

2.1 Synthesis of PBLG-*g*-PEG Graft Copolymers

Materials. Polyethylene glycol monomethyl ether (mPEG-OH) (M_w = 750) was purchased from Sigma Inc. and used without further purification. γ-benzyl-$_L$-glutamate-*N*-carboxyanhydride (BLG-NCA) was synthesized according to literature.[S5-S9] The dialysis bag (Membra-cel, 3500 molecular weight cutoff) was provided by Serva Electrophoresis GmbH. Analytical grades of hexane, tetrahydrofuran (THF), and 1,4-dioxane were refluxed with sodium and distilled immediately before use. All the other reagents are of analytical grade and used as received.

Synthesis of PBLG homopolymer. PBLG homopolymer was synthesized in anhydrous 1,4-dioxane solution using ring-opening polymerization of BLG-NCA initiated by anhydrous trimethylamine.[S10-S11] The reaction was performed in flame-dried reaction bottle under a dry nitrogen atmosphere for 3 days at 15 °C. At the end of the polymerization, the viscous reaction mixture was poured into a large volume of anhydrous ethanol. The precipitated product was dried under vacuum and then purified twice by repeated precipitation from a chloroform solution into a large volume of anhydrous methanol. The weight-average molecular weights (M_w) of the PBLG homopolymers were obtained from the gel permeation chromatography (GPC) analysis (Waters 1515, DMF as eluent solvent), as shown in Table S2.

Synthesis of PBLG-g-PEG graft copolymer. Poly(γ-benzyl-$_L$-glutamate)-*graft*-poly(ethylene glycol) (PBLG-*g*-PEG) graft copolymers were prepared by ester exchange reaction of PBLG homopolymer with mPEG-OH.[S8,S12] The molecular structure and the rod-*g*-coil model of the PBLG-*g*-PEG graft copolymer were illustrated in Figure S2.

The reaction was performed at 55 °C in 1,2-dichloroethane with *p*-toluenesulfuric acid as a catalyst. Then, the reaction mixture was precipitated into a large volume of anhydrous methanol. The product was purified twice by repeated precipitation from a chloroform solution into a large volume of anhydrous methanol and dried under vacuum. The composition of the graft copolymer was determined by ^{1}H NMR spectrum (Avance 550, Bruker) using deuterated chloroform ($CDCl_3$) with 15 vol% deuterated trifluoroacetic acid (TFA-d) as the solvent and tetramethylsilane (TMS) as the internal standard. The degree of grafting is defined as the ratio of the number of PEG chains to the

total degree of polymerization of the polypeptide backbone, which can be calculated from the ratio of the peak intensity of the methylene proton signal (5.1 ppm) of PBLG to that of the ethylene proton signal (3.6 ppm) of PEG in the ^{1}H NMR spectrum (see Figure S2b). By changing the molar ratio of BLG unit to mPEG and the reaction time, the degree of grafting could be adjusted. The GPC traces of the graft copolymers used in this work are shown in Figure S2a. Detailed information regarding the characteristics of these graft copolymers is provided in Table S2.

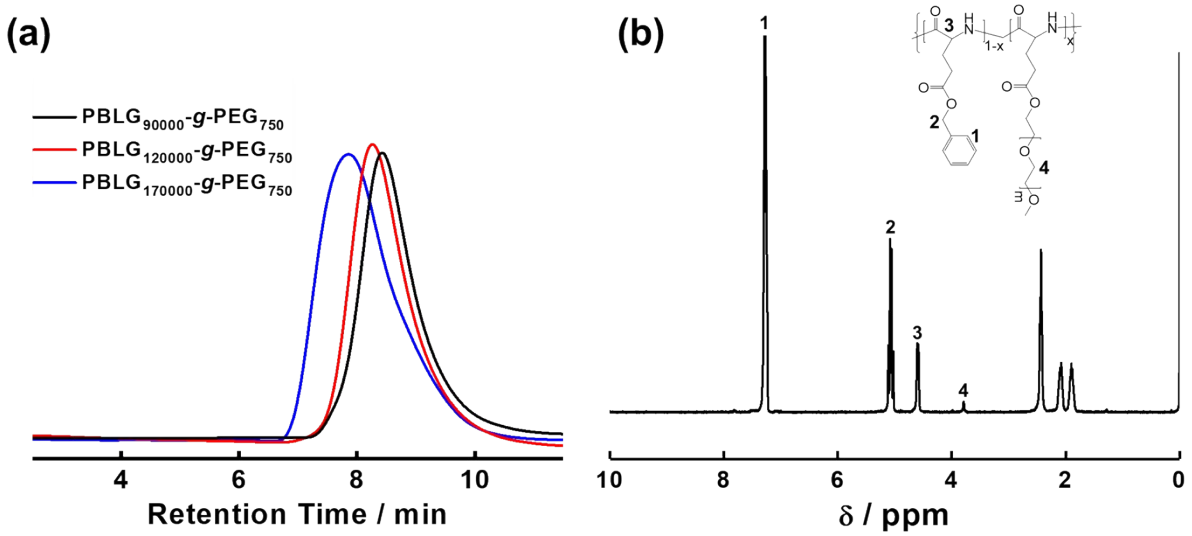

Figure S2. (a) GPC trace of PBLG-*g*-PEG graft copolymers (DMF as eluent solvent). (b) ^{1}H NMR spectra of PBLG-*g*-PEG graft copolymer in $CDCl_3$.

Table S2. Characteristics of PBLG homopolymers and PBLG-*g*-PEG graft copolymers

Sample	$M_{w,PBLG}$[a] (g·mol^{-1})	$M_{w,PEG}$ (g·mol^{-1})	Degree of grafting[b] (%)
$PBLG_{90,000}$	90000	--	--
$PBLG_{120,000}$	120000	--	--
$PBLG_{170,000}$	170000	--	--
$PBLG_{90,000}$-*g*-PEG_{750}	90000	750	0.21
$PBLG_{120,000}$-*g*-PEG_{750}	120000	750	0.19
$PBLG_{170,000}$-*g*-PEG_{750}	170000	750	0.30

[a] The weight-average molecular weight (M_w) of the PBLG homopolymer was obtained from the gel permeation chromatography (GPC) analysis.

[b] The degree of grafting was calculated from the ^{1}H NMR spectrum.

2.2 Preparation of Micelle Solutions

The toroid micelle solution was prepared through a two-step self-assembly process (Scheme S1). In the first-step self-assembly, the cylindrical micelles were prepared using a dialysis method.[S3] The PBLG-*g*-PEG graft copolymers were first dissolved in a THF/DMF (1:1 v/v) solvent mixture (the initial polymer concentration was 0.5 g/L). Then 0.3 mL of deionized water, a selective solvent for PEG, was added to 2.0 mL of polymer solution at a rate of 1.0 mL/min with vigorous stirring. Upon the addition of water, the colorless solution gradually became tint blue, which indicated the formation of aggregates. Finally, the solution was dialyzed against deionized water for 3 days to remove the organic solvents. All experimental procedures, including the processes of adding water and dialysis were performed at a constant temperature (for example 30 °C). In the second-step self-assembly, typically, 1.2 mL of THF was added to 1.0 mL of the cylindrical micelle solution in water with vigorous stir at 30 °C (the resulting THF content is 54.5 vol% in THF/water mixed solvent). The solution was allowed to stir for 24 hours and then dialyzed against water to remove THF.

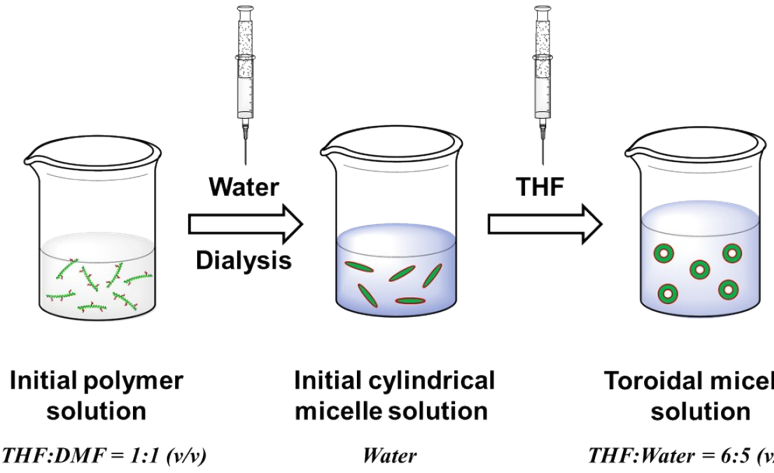

Scheme S1. Schematic representation of the micellar solution preparation through a two-step self-assembly process.

2.3 Characterization of Assemblies

Scanning Electron Microscopy (SEM). The surface profile of the aggregates was obtained from Field Emission SEM (S4800, Hitachi) operated at an accelerating voltage of 15 kV. The sample was prepared by placing drops of solution on a copper grid coated with carbon film (or freshly cleaned silicon wafer) and then drying the solution under proper temperature. Before observation, the samples were sputtered by gold.

Transmission Electron Microscopy (TEM). The morphologies of toroidal micelles were examined by TEM (JEM-2100F, an accelerating voltage of 200 kV). Drops of micelle solution were placed on a copper grid coated with carbon film and then was dried at room temperature.

Atom Force Microscopy (AFM). AFM measurements were performed with XE-100 system (Park Systems) by using the non-contact mode at room temperature in air. The samples were prepared by placing drops of solution on a fresh-cleaved mica surface and then drying the solution at room temperature.

Synchrotron Radiation X-ray Scattering. The solution of cylindrical and toroidal micelles formed by $PBLG_{170000}$-*g*-PEG_{750} was vacuum-dried at room temperature to obtain a powder sample for the synchrotron radiation small-angle X-ray scattering (SAXS) and wide-angle X-ray scattering (WAXS) measurements. SAXS and WAXS measurements were performed at beamline BL16B of Shanghai Synchrotron Radiation Facility. The wavelength of X-ray is 0.124 nm and the distance of the sample to the detector is 180 mm for WAXS (1948 mm for SAXS) measurement. The *d*-spacing values are calculated from Bragg's Law. Two-dimensional SAXS and WAXS patterns are collected with a Mar165 CCD detector (2048 × 2048 pixels with a pixel size of 172 μm). The SAXS and WAXS data are analyzed with Fit2D software from the European Synchrotron Radiation Facility.

3. Theory of Supramolecular Cyclization

3.1 Thermodynamic Condition

The free energy of cylindrical micelle is comprised of the chain conformational energy, the interfacial energy, and the end-cap energy.[S13-14] To describe the cyclization process of cylindrical micelles with semiflexible copolymer backbones, we considered the contribution of the bending energy to the total energy and then developed the theory of supramolecular cyclization.

We first write the energy function of cylindrical micelles and then obtain the thermodynamic condition of the interfacial energy and the backbone rigidity for the supramolecular cyclization. We simplify the cylindrical micelle into a spherocylinder model, as shown in Figure S3. The length and diameter of cylindrical micelle are denoted as L and D, respectively. The rigid backbones of graft copolymers take a parallel packing to form the micellar core, and the partially exposed ends were represented by two hemispheres (see Figure S3).

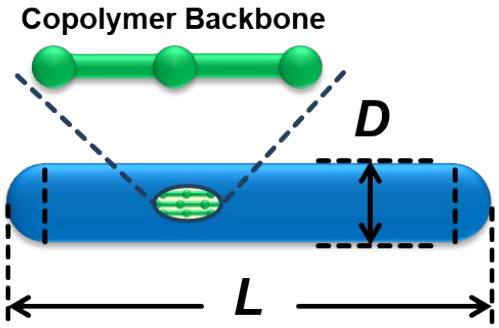

Figure S3. Sketch of the cylindrical micelle assembled from rod-coil graft copolymers.

The interfacial energy of the initial cylindrical micelle was denoted as E_{inter}. Due to the ordered packing of copolymer backbones in the core, the cylindrical micelle is rodlike structure, that is, the radius of curvature tends to infinity. Thus, the bending energy of cylindrical micelle E_{bend} approximates to 0. In addition, the end-cap energy was denoted as E_{end}, which was regarded as constant in the cyclization process. Therefore, the total energy E_{cylinder} of the cylindrical micelle can be written as

$$E_{\text{cylinder}} = E_{\text{inter}} + E_{\text{bend}} + 2E_{\text{end}} \quad \text{(S-6)}$$

The sketch of the curved micelle bent from cylindrical micelle is shown in Figure S4. The radius of curvature and the bending angle of curvature are defined as R and φ, respectively. Noted

that the interfacial energy E_{inter} and the bending energy E_{bend} are the functions of R, while the end-cap energy E_{end} is unchanged.[S13-S14] Thus, the total energy E_{curved} of curved micelle can be written as

$$E_{\text{curved}}(R) = \Delta E_{\text{inter}}(R) + \Delta E_{\text{bend}}(R) + E_{\text{cylinder}} \tag{S-7}$$

where Δ denotes the energy variation from cylinder to curved micelle. Thus, the energy E_{curved} achieves minimum at R^* which satisfies the following relationship

$$\left.\frac{\partial E_{\text{curved}}(R)}{\partial R}\right|_{R=R^*} = \left.\frac{\partial \Delta E_{\text{inter}}(R)}{\partial R}\right|_{R=R^*} + \left.\frac{\partial \Delta E_{\text{bend}}(R)}{\partial R}\right|_{R=R^*} = 0 \tag{S-8}$$

Therefore, when the functions of the interfacial energy and the bending energy are given out, the equilibrium state of the curved micelle and the bend angle or the radius of curve can be obtained from Eq.S-8.

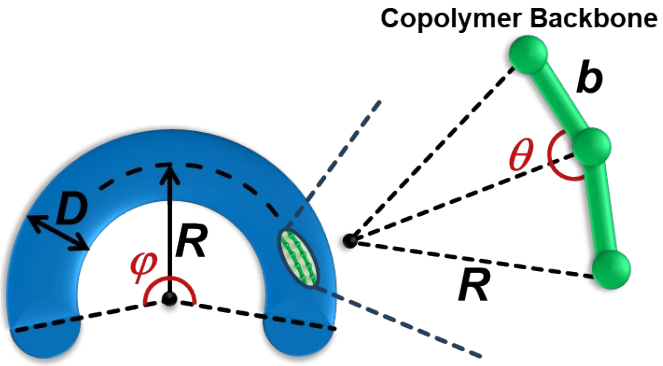

Figure S4. Sketch of the curved micelle bended from cylindrical micelle and the bending angle of rigid backbones in the curved micellar core.

The backbones are bended in the core of curved micelle, as shown in Figure S4. We defined the length of the bond on the backbone as b and the length of bond connecting backbone bead and pendant group is c. If the average value of the bending angle for the rigid backbone is denoted as $\langle\theta\rangle$, we can obtain the approximated relation of $\cos\left(\frac{\langle\theta\rangle}{2}\right) = \frac{b}{2R}$. The bending energy of cylindrical micelle can be estimated by summing the bending angle potential of the backbones in the micelle core.[S15-S16] The bending angle potential of semiflexible chains, for example, DNA chains, is given by $E_{\text{bend}} = \frac{1}{2} g_b \beta^2$, where g_b is a stiffness constant related to the bending persistence length, and β is the angle between the tangent vectors of the neighboring chain segments.[S16] Employing this model to

the semiflexible backbones in our work, the bending energy variation ΔE_{bend} of the curved micelle is written as

$$\Delta E_{\text{bend}} = N\frac{k}{2}\left\langle\left(\theta-\theta_0\right)^2\right\rangle \approx N\frac{k}{2}\left(\left\langle\theta\right\rangle-\theta_0\right)^2 \tag{S-9}$$

where N is the bead number of backbones in the core, k is the stiffness of backbones, and θ_0 is the equilibrium angle between the neighboring bonds.

From Figure 3, we learn that the variation of the interaction between pedant groups (*i.e.* **P−P** interaction) mainly contributes to the variation of interfacial energy and thereby the cyclization process. Therefore, we only evaluate the interaction energy variation ΔE_{PP} during the cyclization process to describe the variation ΔE_{inter}. This pairwise **P−P** interaction could be described by the standard Lennard-Jones (LJ) potential (Eq.S-3), which is numerically close to the more realistic Morse potential of nonbonded attractive interaction.[S16-S17] According to the bending angle of backbone, the average distance between the neighboring **P** beads on the backbone can be estimated to be $b-2c\cos\left(\frac{\left\langle\theta\right\rangle}{2}\right)$, and thus the variation of the average **P−P** interaction energy can be written with LJ potential equation

$$\Delta E_{\text{PP}} = 4N\varepsilon_{\text{PP}}\left[\left(b-2c\cos\left(\frac{\left\langle\theta\right\rangle}{2}\right)\right)^{-12}-\left(b-2c\cos\left(\frac{\left\langle\theta\right\rangle}{2}\right)\right)^{-6}-\left(r_{\text{PP}}^{c}\right)^{-12}+\left(r_{\text{PP}}^{c}\right)^{-6}\right] \tag{S-10}$$

where ε_{PP} and r_{PP}^{c} is the interaction strength and the cut-off distance between **P** beads. Thus, the total energy of curved micelles can be obtained from

$$\begin{aligned} E_{\text{curved}} &= \Delta E_{\text{bend}} + \Delta E_{\text{inter}} + E_{\text{cylinder}} \approx \Delta E_{\text{bend}} + \Delta E_{\text{PP}} + E_{\text{cylinder}} \\ &= \frac{k}{2}N\left(\left\langle\theta\right\rangle-\theta_0\right)^2 + 4N\varepsilon_{\text{PP}}\left[\left(b-2c\cos\left(\frac{\left\langle\theta\right\rangle}{2}\right)\right)^{-12}-\left(b-2c\cos\left(\frac{\left\langle\theta\right\rangle}{2}\right)\right)^{-6}-\left(r_{\text{PP}}^{c}\right)^{-12}+\left(r_{\text{PP}}^{c}\right)^{-6}\right] + E_{\text{cylinder}} \end{aligned} \tag{S-11}$$

We seek the optimal configuration by minimizing this energy with respect to $\left\langle\theta\right\rangle$, that is,

$$\left.\frac{\partial E_{\text{curved}}}{\partial\left\langle\theta\right\rangle}\right|_{\left\langle\theta\right\rangle=\left\langle\theta\right\rangle^*} = 0, \qquad \left.\frac{\partial^2 E_{\text{curved}}}{\partial\left\langle\theta\right\rangle^2}\right|_{\left\langle\theta\right\rangle=\left\langle\theta\right\rangle^*} > 0 \tag{S-12}$$

This minimization leads to the optimal thermodynamic condition which satisfies

$$\varepsilon_{\mathrm{PP}} = \frac{k\left(\left\langle\theta\right\rangle^{*} - \theta_0\right)}{48c\sin\left(\frac{\left\langle\theta\right\rangle^{*}}{2}\right)\left(b - 2c\cos\left(\frac{\left\langle\theta\right\rangle^{*}}{2}\right)\right)^{-13} - 24c\sin\left(\frac{\left\langle\theta\right\rangle^{*}}{2}\right)\left(b - 2c\cos\left(\frac{\left\langle\theta\right\rangle^{*}}{2}\right)\right)^{-7}} \quad \text{(S-13)}$$

For a given interaction strength $\varepsilon_{\mathrm{PP}}$ and the backbone rigidity k, the optimal angle for the backbone $\left\langle\theta\right\rangle^{*}$ can be obtained from Eq. S-13. Combining with $\cos\left(\frac{\left\langle\theta\right\rangle^{*}}{2}\right) = \frac{b}{2R^{*}}$, we can obtain the optimal radius of curved micelle R^{*}.

As $\left\langle\theta\right\rangle^{*} = \theta_0 = 180°$, the morphology is cylindrical micelle with the parallel packing of rigid backbones within the micelle core. In this case, the bend energy U_{bend} vanishes. As $\left\langle\theta\right\rangle^{*}$ is $2\arccos\left(\frac{b}{2R_{\mathrm{tor}}}\right)$, the toroidal micelle is formed, where R_{tor} is the radius of toroid. Therefore, $\left\langle\theta\right\rangle^{*}$ should satisfy the condition of $2\arccos\left(\frac{b}{2R_{\mathrm{tor}}}\right) < \left\langle\theta\right\rangle^{*} < 180°$.

3.2 Geometric Condition

Figure S5 shows the sketch of the toroidal micelles cyclized from cylindrical micelles. The radius of the toroid and the diameter of the toroidal cylinder are denoted as R_{tor} and d_{tor}, respectively.

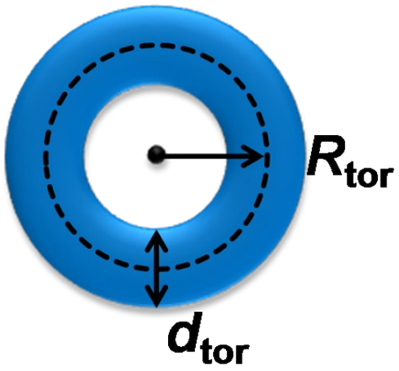

Figure S5. Sketch of the toroidal micelle cyclized from cylindrical micelle.

At the moment of end-to-end closure, the circumference of toroidal micelle is equal to the length of cylindrical micelle, *i.e.*, $L = 2\pi R_{tor}$. The diameter of the toroidal cylinder is close to the diameter of the initial cylinder (*i.e.* $D = d_{tor}$). Because the hole in the center of toroid is a necessary geometric feature, the diameter of toroid should be larger than the diameter of toroidal cylinder, that is,

$$2R_{tor} - d_{tor} > 0 \quad \Rightarrow \quad 2R_{tor} > d_{tor} \tag{S-14}$$

Thus, we can obtain a geometric condition for the end-to-end closure as

$$L / D = \frac{2\pi R_{tor}}{d_{tor}} > \pi \tag{S-15}$$

This means that the aspect ratio L/D of the pre-assembled cylinders have to be larger than π to cyclize into a toroid.

4. Effect of Backbone Rigidity on Morphologies of Toroidal Micelles

The backbone rigidity is described by the angle spring constant k in the angle potential. As the k value decreases, the backbone becomes flexible. As the k is 20ε, toroid micelles cyclized from cylindrical micelles were observed. Figure S6a displays the density profiles of backbone and side chain along the diameter of toroid. For the core-forming backbones (green curve), the profile displays a bimodal feature, while the profile of the corona-forming side chain (red curve) shows four peaks, which confirm the toroidal structures. With decreasing the k value to 10ε, a toroidal micelle with the smaller hole was observed (see Figure S6b). Further decreasing the k (5.0ε), spherical micelles consisting of core formed by flexible backbones and corona formed by side chains were obtained (see the inset of Figure S6c). The unimodal distribution of the backbones and the bimodal distribution of side chain demonstrate the spherical structure. The simulation results are consistent with our previous experimental observations, that is, toroidal micelles collapse into ellipsoidal and spherical structures when decreasing the PBLG backbone rigidity.[S5] The results indicate that the rigidity of the polymer backbones plays an important role in the formation of toroidal structures.

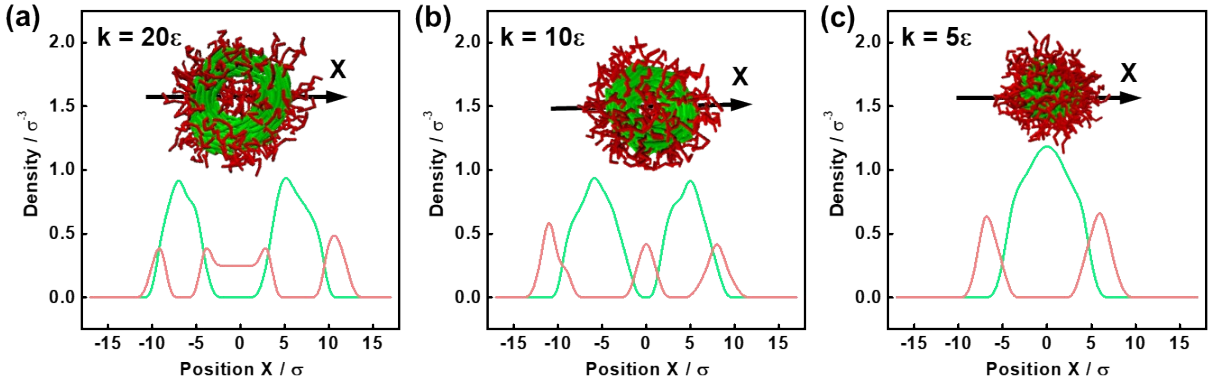

Figure S6. (a-c) Density profiles along the X-axis of micelles obtained at various backbone rigidities. The green and the red curves are the density distribution of backbones and side chains, respectively.

5. Effect of Aspect Ratio of Cylindrical Micelle

It has been revealed that the cylindrical micelle should stratify an appropriate aspect ratio *L/D* for the end-to-end closure cyclization, *i.e.* $L/D > \pi$. Herein, in order to further verify this condition, we decrease the length of the polymer backbones to obtain the micelle with a lower aspect ratio and then try to induce its cyclization by increasing the interaction strength ε_{PP} between pendant groups. The results are shown in Figure S7. Compared with the micelle morphologies shown in Figure 5, the shorter cylindrical micelles are assembled from the graft copolymers with shorter backbones, $\mathbf{R}_6$-*g*-$(\mathbf{C}_6)_2$ (see Figure S7a). The polydisperse distribution of aspect ratio was shown in Figure S7b, and the aspect ratio of 95% cylindrical micelle is below the critical value π. After enhancing the interaction strength ε_{PP} to 5.0ε, these micelles cannot transform into curved or toroidal micelles and remain the cylindrical structure (see Figure S7c). Noted that the aspect ratio decreases slightly due to the higher interfacial energy caused by increasing ε_{PP} (see Figure S7d). Even if we further increase the interaction strength ε_{PP} to 7.0ε, the short micelles still cannot be bended or cyclize into toroids, and the aspect ratio further decreases (see Figure S7e-f). The simulation results further support the proposed geometric condition ($L/D > \pi$) for this supramolecular cyclization.

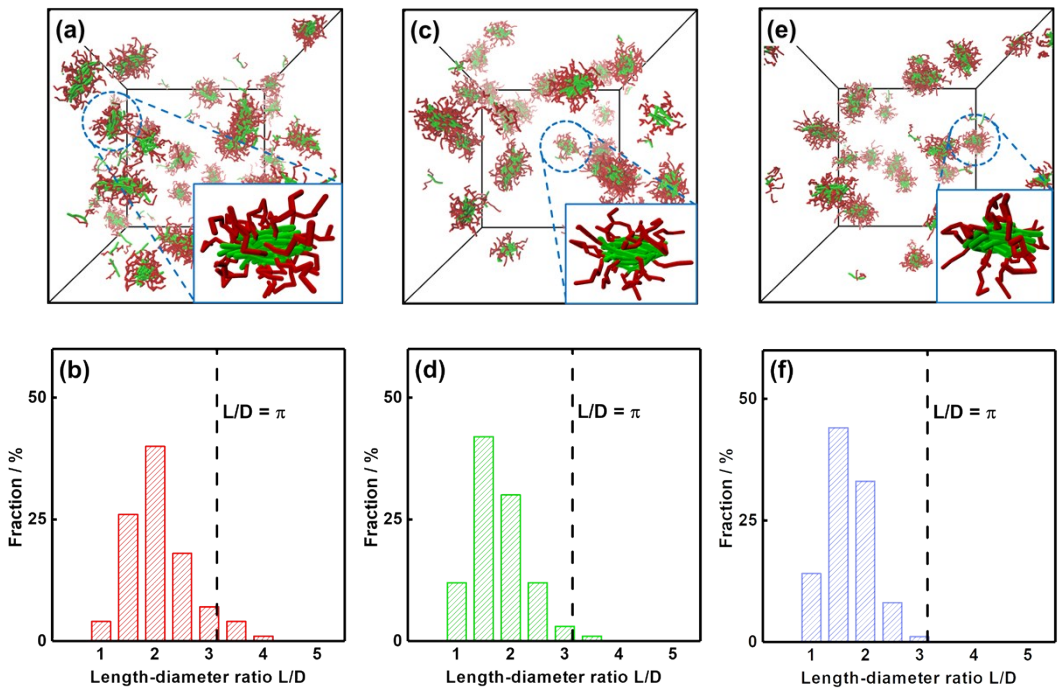

Figure S7. (a, c, e) Simulation morphologies of (a) cylindrical micelles assembled from copolymer $\mathbf{R}_6$-*g*-$(\mathbf{C}_6)_2$ and (c, e) aggregates after increasing the interaction strength ε_{PP} to (c) 5.0ε and (e) 7.0ε. (b, d, f) Distributions of the aspect ratio *L/D* for the micelle structures in (a), (c) and (e), respectively.

In the experiment, the cylindrical micelles with the lower aspect ratio ($L/D = 0.92\pi$) are formed by $PBLG_{90,000}$-*g*-PEG_{750} graft copolymers, these cylindrical micelles cannot be bended into curved micelle after adding 1.2 ml of THF into 1.0 mL of micelle solution. Here, we further increase the THF content to examine whether these shorter cylindrical micelles can transform into curved or toroidal micelles. 2.0 mL and 3.0 mL of THF were added into 1.0 mL of micelle solution, and the THF contents reach 66.7 vol% and 75.0 vol%, respectively. SEM images of the aggregates obtained from these two groups of micelle samples were shown in Figure S8. Only the cylindrical micelle morphology can be observed. That is, even if we further increase the THF content, curved or toroidal structures still cannot be observed. The results indicate that the geometric condition ($L/D > \pi$) is necessary for the supramolecular cyclization.

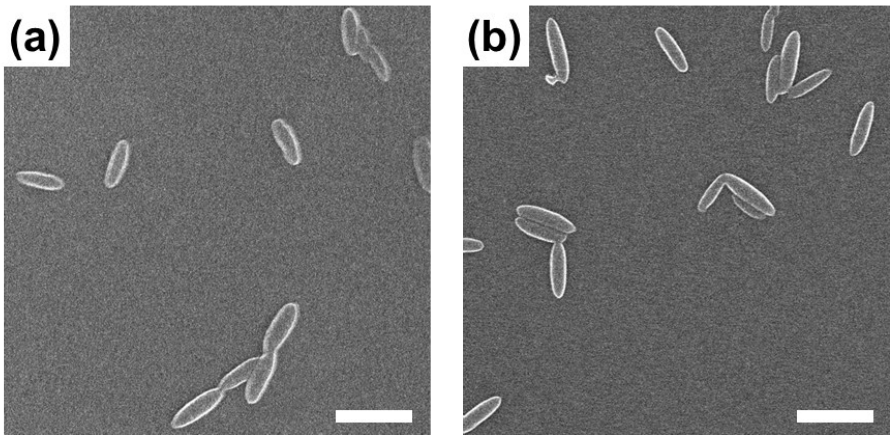

Figure S8. SEM images of aggregates obtained by adding (a) 2.0 mL and (b) 3.0 mL of THF into 1.0 mL of the solution of pre-assembled cylindrical micelles formed by $PBLG_{90,000}$-*g*-PEG_{750} graft copolymers. Scale bars: 500 *nm*.

6. TEM and AFM Measurements of Toroidal Micelles

To further confirm the morphologies of toroidal micelles, we carried out TEM and AFM measurements on the toroids transformed from cylindrical micelles of $PBLG_{170000}$-*g*-PEG_{750}. The TEM and AFM images of the toroids are shown in Figure S9a and Figure S9b, respectively. The morphologies and the diameter of toroids in TEM and AFM images are found to be consistent with those in the SEM results shown in Figure 6. Therefore, TEM and AFM results further confirm the morphologies of toroidal micelles.

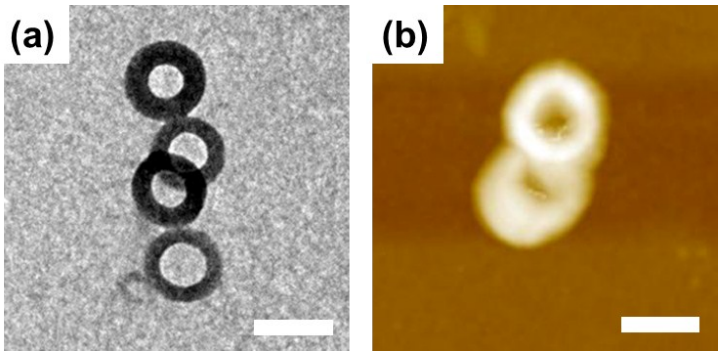

Figure S9. (a) TEM and (b) AFM images of toroidal micelles cyclized from cylindrical micelles of $PBLG_{170000}$-*g*-PEG_{750}. Scale bar: 300 *nm*.

7. Effect of the Length of Side Chains

Here, we performed simulations for the graft copolymers with various lengths of coil side chains to evaluate the effect of PEG molecular weight. The representative simulation results of cylindrical micelles formed by $\mathbf{R}_{10}$-*g*-$(\mathbf{C}_4)_2$, $\mathbf{R}_{10}$-*g*-$(\mathbf{C}_6)_2$, and $\mathbf{R}_{10}$-*g*-$(\mathbf{C}_8)_2$ were given in the inset of Figure S10. The average aspect ratios of these assemblies were calculated from five groups of independent simulations. As shown in Figure S10, with increasing the **C** graft length (L_c), the cylindrical structure can maintain, but the aspect ratio of micelles gradually decreases. The results imply that in addition to the molecular weight of PBLG backbones, the molecular weight of PEG chains can also affect the aspect ratio of cylindrical micelles. The suitable molecular weight of PEG is necessary to guarantee that the aspect ratio of micelles can satisfy the geometric condition for cyclization. As the length L_c of **C** side chains is sufficiently long, the aspect ratio *L*/*D* of micelles cannot satisfy the geometric condition for cyclization (*i.e.* $L/D > \pi$; the dashed line in Figure S10). The simulations are consistent with the experimental observations about the effect of PEG molecular weight on the aggregate morphology in our previous work.[S12,S19]

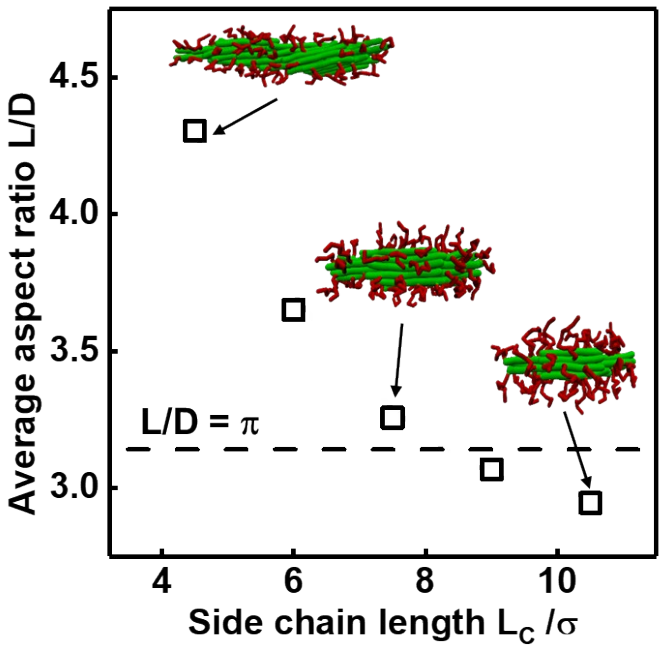

Figure S10. Variation of the average aspect ratio *L*/*D* for cylindrical micelles assembled from graft copolymers with various side chain lengths L_c. The bead number of rigid backbones is 10, and the interaction parameters are $\varepsilon_{RR} = 3.5\varepsilon$ and $\varepsilon_{PP} = 1.0\varepsilon$.

8. Synchrotron Radiation SAXS and WAXS Results of Cylindrical and Toroidal Micelles

To obtain the microstructural characteristics of cylindrical and toroidal micelles, we carried out synchrotron radiation SAXS and WAXS measurements on the micelle samples. The aqueous solutions of cylindrical and toroidal micelles formed by $PBLG_{170000}$-*g*-PEG_{750} were vacuum-dried at room temperature to prepare powder samples. The SAXS and WAXS diffraction patterns are shown in Figure S11. The microstructural size of micelles and the periodically ordered structure in the micelles can be obtained from the SAXS (Figure S11a-b) and WAXS results (Figure S11c-d), respectively.[S20-S22] The SAXS and WAXS spectra were calculated from the 2D diffraction patterns with Fit2D software (see Figure S11e-f). As shown in Figure S11e, a sharp diffraction peak appears at q = 0.066 nm^{-1} for cylindrical micelles and q = 0.063 nm^{-1} for toroidal micelles. In terms of Bragg's Law, the distance d of the ordered periodic nanostructures is given by $d = 2\pi/q$. The values of d for the cylindrical micelles and toroidal micelles are 95.2 nm and 99.7 nm, respectively. 95.2 nm and 99.7 nm are considered as the diameter of cylinder and the diameter of the toroidal cylinder, respectively, which is consistent with the SEM and TEM results of cylindrical and toroidal micelles.

In the WAXS spectra of cylindrical and toroidal micelle samples (Figure S11f), there are two major diffraction peaks near 3.9 nm^{-1} and 12.7 nm^{-1}. The values of d for these two peaks are 1.61 nm ($2\pi/3.9$) and 0.49 nm ($2\pi/12.7$), respectively. 1.61 nm is considered as the distance between two parallel packing PBLG backbones,[S20,S21] and 0.49 nm is considered as the helical pitch of PBLG with α-helix conformation (note that the length is 0.54 nm for the standard α-helix conformation).[S22] The WAXS results indicate that the PBLG backbones take an ordered packing manner in the micellar core, which is consistent with the theoretical simulations. Note that the parallel packing of PBLG backbones (*i.e.* the diffraction peak at 3.81 nm^{-1}) can maintain during the cyclization of cylindrical micelles.

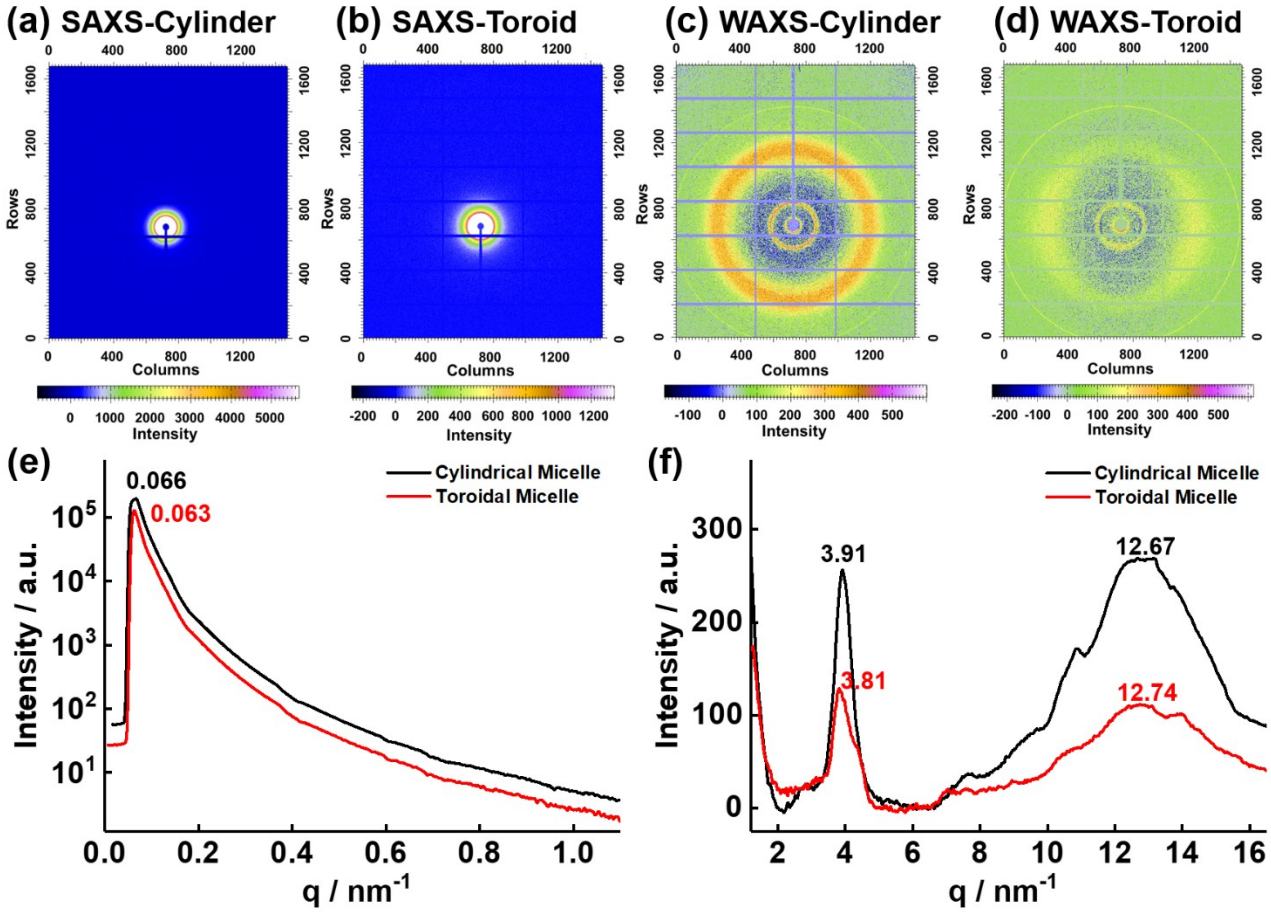

Figure S11. Synchrotron radiation (a-b) SAXS and (c-d) WAXS diffraction patterns for the power samples of cylindrical and toroidal micelles, respectively. (e) SAXS and (f) WAXS spectra of the micelle samples.

References

[S1] LAMMPS home page. http://lammps.sandia.gov.

[S2] G. S. Grest, K. Kremer, *Phys. Rev. A* **1986**, *33*, 3628-3631.

[S3] S. Lin, N. Numasawa, T. Nose, J. Lin, *Macromolecules* **2007**, *40*, 1684-1692.

[S4] M. A. Horsch, Z. Zhang, S. C. Glotzer, *Phys. Rev. Lett.* **2005**, *95*, 056105.

[S5] C. Yang, L. Gao, J. Lin, L. Wang, C. Cai, Y. Wei, Z. Li, *Angew. Chem. Int. Ed.* **2017**, *56*, 5546-5550.

[S6] E. R. Blout, R. H. Karlson, *J. Am. Chem. Soc.* **1956**, *78*, 941-946.

[S7] C. Cai, L. Zhang, J. Lin, L. Wang, *J. Phys. Chem. B* **2008**, *112*, 12666-12673.

[S8] Z. Zhuang, T. Jiang, J. Lin, L. Gao, C. Yang, L. Wang, C. Cai, *Angew. Chem. Int. Ed.* **2016**, *55*, 12522-12527.

[S9] C. Yang, Q. Li, C. Cai, J. Lin, *Langmuir* **2016**, *32*, 6917-6927.

[S10] C. Cai, Y. Li, J. Lin, L. Wang, S. Lin, X.-S. Wang, T. Jiang, *Angew. Chem. Int. Ed.* **2013**, *52*, 7732-7736.

[S11] C. Cai, J. Lin, X. Zhu, S. Gong, X.-S. Wang, L. Wang, *Macromolecules* **2016**, *49*, 15-22.

[S12] C. Cai, J. Lin, T. Chen, X. Tian, *Langmuir* **2010**, *26*, 2791-2797.

[S13] S. May, Y. Bohbot, A. Ben-Shaul, *J. Phys. Chem. B* **1997**, *101*, 8648-8657.

[S14] M. Asgari, *Eur. Phys. J. E* **2015**, *38*, 98.

[S15] T. X. Hoang, A. Giacometti, R. Podgornik, N. T. T. Nguyen, J. R. Banavar, A. Maritan *J. Chem. Phys.* **2014**, *140*, 064902.

[S16] R. Cortini, B. R. Caré, J. M. Victor, M. Barbi, *J. Chem. Phys.* **2015**, *142*, 105102.

[S17] L. Cheng, J. Yang, *J. Chem. Phys.* **2007**, *127*, 124104.

[S18] O. Cauchoisa, F. Segura-Sanchezb, G. Ponchela, *Int. J. Pharm.* **2013**, *452*, 292.

[S19] H. Gao, X. Ma, J. Lin, L. Wang, C. Cai, L. Zhang, X. Tian, *Macromolecules* **2019**, *52*, 7731.

[S20] A. Schmidt, S. Lehmann, M. Georgelin, G. Katana, K. Mathauer, F. Kremer, K. Schmidt-Rohr, C. Boeffel, G. Wegner, W. Knoll, *Macromolecules* **1985**, *28*, 5487.

[S21] L. Wang, Y. Huang, *Macromolecules* **2004***, 37*, 303.

[S22] H. Y. Tang, C. U. Lee, D. H. Zhang, *J. Polym. Sci. A Polym. Chem.* **2011***, 49*, 3228.